Small Signal and Microscopic Noise Simulation of an nMOSFET by a Self-Consistent, Semi-Classical and Deterministic Approach

Dino Ruić* and Christoph Jungemann
Chair of Electromagnetic Theory
RWTH Aachen University
52056 Aachen, Germany
*Email: dr@ithe.rwth-aachen.de

***Abstract*—We present fully self-consistent small signal and microscopic noise simulations of a nanoscale double-gate nMOSFET by a semi-classical and deterministic approach. We show how such a system of Poisson, Schrödinger and Boltzmann equations can be used to self-consistently determine several key quantities relevant to circuit designers.**

I. Introduction

Semi-classical simulations based on the Poisson equation (PE), Schrödinger equation (SE) and Boltzmann equation (BE) are an important tool to understand the intricacies of nanoscale MOSFETs with feature sizes of just a few nanometers.

A typical scheme to solve these equations for the stationary case is a Gummel type iteration where all three equations are solved separately, one after the other, until convergence is achieved [1]. For RF calculations, this scheme becomes problematic since the response of the device to a fluctuation or an exterior perturbation is not solely based on one equation but on the interplay of all equations that describe the state of the device. It becomes a necessity to treat the PE, SE and BE as a fully coupled system of equations that should be solved self-consistently or else the results might have infeasibly large errors [2].

Deterministic solvers of the BE based on the expansion of $\boldsymbol{k}$-space in spherical harmonics [3] or Fourier harmonics [4] are well suited to be adapted into such a simultaneous solver. To this end, much of the work needs to be invested into ensuring that all physical properties in the continuum are satisfied in the simulator on a discrete grid. For example, it is by no means obvious that a property like reciprocity in equilibrium, which is essentially a symmetry relation between the PE and BE, is fulfilled on a finite grid.

This work is based on the efforts in Ref. [2] where the numerical methods have been developed to achieve a simultaneous solver for the full system of equations of the PE, SE, and BE that ensures small signal current conservation as well as reciprocity, passivity, and the Nyquist theorem in equilibrium. We will show how such a simulator can be used to compute important small signal and noise quantities for circuit design for a wide range of bias conditions and frequencies.

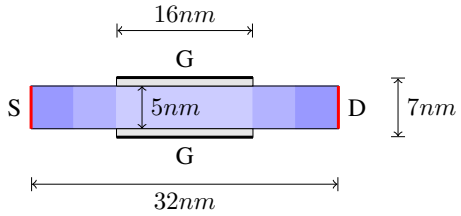

Fig. 1. Double gate nMOSFET with a silicon channel. The shades in the channel indicate the doping density N_D.

II. Approach

We consider the two-dimensional device of Fig. 1 which is treated as translationally invariant in the third dimension. Our semi-classical approach involves solving the two-dimensional PE, the BE in transport direction from source to drain with a parabolic band structure, and the SE in confinement direction (perpendicular to transport). In order to solve the BE deterministically, we use the Herring-Vogt transformation [5], the Fourier harmonics expansion [4], and the H-transformation [3]. Scattering includes the Pauli principle and comprises elastic acoustic phonon scattering and inter-valley phonon scattering [6] as well as surface roughness scattering by a Prange-Nee term [7] in the velocity-randomizing approximation [8].

To obtain stationary solutions, we use the quadratically converging Newton-Raphson approach to simultaneously solve the PE, SE, and BE [9].

Small signal quantities can be evaluated self-consistently by a linearization around the stationary values of the PE, SE, and BE. However, difficulties arise due to the discretization on a finite grid. Results from a naive implementation of such a linearization will not be reciprocal or passive in equilibrium but careful considerations can be used to restore necessary symmetries between the BE and PE [2].

Likewise, noise quantities can be described by small fluctuations and hence by a linearization of the PE, SE, and BE. We use the Langevin-source approach (see e.g. [10]) to describe fluctuations in terms of Green's functions and solve the whole system of equations by the adjoint method [11] for the Green's functions of terminal currents. Computation of the terminal currents requires an adequate formulation of the

978-1-4673-7860-4/15/$31.00 ©2015 IEEE

Ramo-Shockley theorem [12]–[14] that is valid for our model, i.e. two-dimensional PE, SE in confinement direction and BE in transport direction. This leads to non-trivial difficulties that need to be addressed in order to obtain a sound definition of terminal currents as was discussed in great detail in Ref. [2].

The Green's functions are used to compute the power spectral density (PSD) of the fluctuations of terminal currents [10] with the noise sources given by generation/recombination rates at the contacts and scattering. That means, there are no further degrees of freedom for the full calculation of the noise in a device.

Small signal related figures of merit include the cut-off frequency and the maximum oscillation frequency which are properties of the hybrid parameters and the unilateral gain, respectively. Both are easily computed if the admittance parameters are known.

The noise characterization of a MOSFET in common-source configuration involves a set four figures of merit that describe the noise of the device for circuit designers [15]. These may be given as the minimum noise figure $F_{\min}$, the noise resistance R_{N}, and real and imaginary parts of the optimum generator admittance Y_{opt}. However, other representations are possible which might be better suited to manifest certain features.

In this work, we will focus on the wide-spread representation of the noise characteristics in terms of the cross-correlation and the drain/gate excess noise factors. The cross-correlation is given by

$$c = \frac{W_{12}}{\sqrt{W_{11}W_{22}}} \tag{1}$$

and the gate and drain excess noise factors are [16], [17]

$$\beta = \frac{5W_{11}g_{\mathrm{D0}}}{4k_BT(\omega C_{\mathrm{GS}})^2}, \qquad \gamma = \frac{W_{22}}{4k_BTg_{\mathrm{D0}}}, \tag{2}$$

respectively. Here, W_{ij} is the PSD of terminal currents. The index '1' corresponds to the gate while '2' corresponds to the drain of our device in common-source configuration. The parameter g_{D0} is given by the drain self-admittance at zero drain bias and zero frequency and ωC_{GS} was approximated via

$$\omega C_{\mathrm{GS}} \approx \mathrm{Im}(Y_{11} + Y_{12}),$$

which is valid for not too high frequencies, i.e. while Y_{11} and Y_{12} are still linear in frequency (cf. Fig. 4).

III. Results

We investigate a two-dimensional double-gate nMOSFET with a silicon channel in common-source configuration as shown in Fig. 1. All results in the remainder of this work refer to the intrinsic device. Parasitics (e.g. gate resistance) are neglected.

We use a grid point spacing of $0.2nm$ in confinement direction and $0.5nm$ in transport direction while the energy grid has a spacing of $2.6meV$. The number of subbands was limited to the 10 lowest ones and the Fourier harmonics expansion was truncated beyond the 7th order. In total we have anywhere between 1.3 to 1.8 million unknowns, depending on the operating point. This necessitates around 250GB of memory and solving for the stationary solution of a single operating point takes anywhere between 2h and 10h wall clock time on a work station with two 8-core Intel Xeon E-2690 processors.

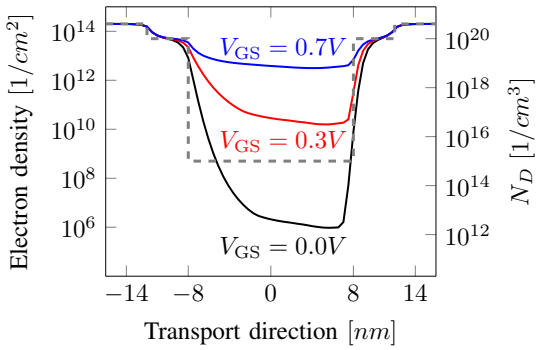

Fig. 2. Electron density in transport direction (solid lines, left axis) for $V_{GS} = 0.0V$, $0.3V$, $0.7V$ at $V_{DS} = 0.7V$ as well as the donor doping density N_D (dashed line, right axis).

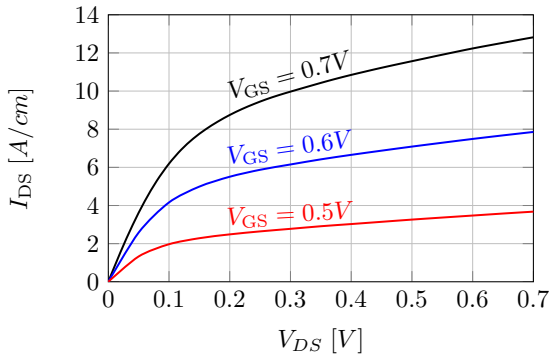

Fig. 3. Stationary drain current I_{DS} vs. drain bias at $V_{GS} = 0.5V$, $0.6V$, $0.7V$.

Figure 2 shows the resulting stationary electron density within the device along the transport direction for various gate biases and Fig. 3 depicts the current-voltage curves.

Small signal and microscopic noise evaluation can be done with only one solution step by reusing the Green's functions of terminal currents. Thus, at a single operating point and frequency, both small signal parameters and Green's functions of terminal currents can be computed within an hour, while the evaluation of the PSD takes another 15 minutes.

A. Small Signal Analysis

The small signal analysis yields small signal current conserving results and is reciprocal and passive in equilibrium. Figure 4 shows the admittance parameters versus frequency at $V_{GS} = 0.7V$ and $V_{DS} = 0V$, i.e. in equilibrium. For a two-port in equilibrium $Y_{12} = Y_{21}$ must hold for it to be reciprocal and the figure indicates that this is indeed fulfilled.

The admittances versus the gate bias for $V_{DS} = 0.7V$ are shown in Fig. 5. With the admittance parameters, we can compute cut-off frequencies and maximum oscillation frequencies for various operating points as shown in Fig. 6. The maximum oscillation frequency is rather high because the

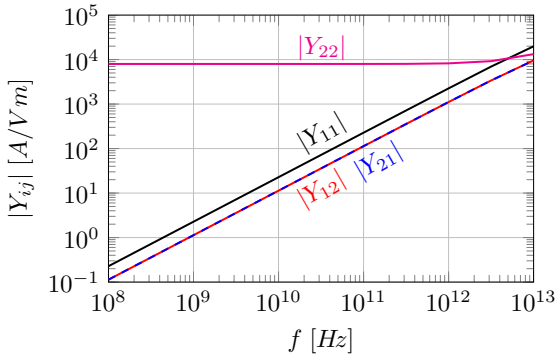

Fig. 4. Absolute value of admittance parameters $|Y_{ij}|$ (as indicated) vs. frequency at $V_{GS} = 0.7V$ and $V_{DS} = 0.0V$. Note that $|Y_{12}|$ (red) is equal to $|Y_{12}|$ (blue) which is to be expected if reciprocity is fulfilled in equilibrium

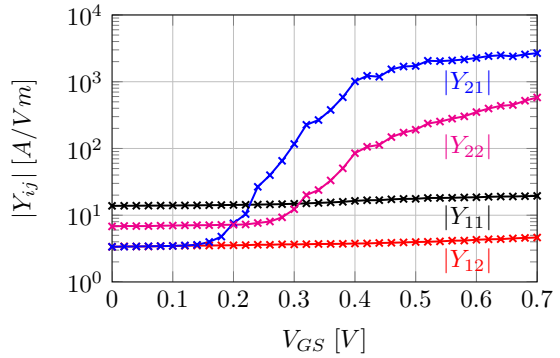

Fig. 5. Absolute value of admittance parameters $|Y_{ij}|$ (as indicated) vs. gate bias V_{GS} at $V_{DS} = 0.7V$ and $10GHz$.

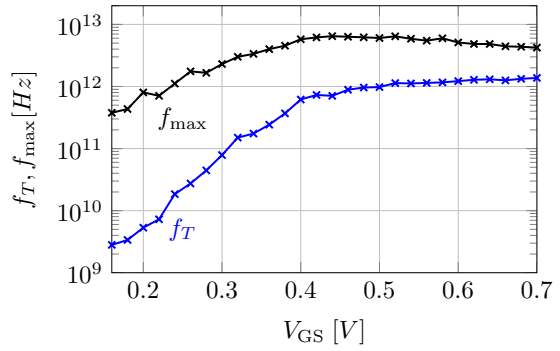

Fig. 6. Cut-off frequency f_T (blue) and maximum oscillation frequency $f_{\max}$ (black) vs. gate bias.

device simulation contains neither a gate resistance nor other parasitics present in real devices.

In both, Fig. 5 and Fig. 6, discontinuities can be seen which are artifacts of discretization that occur whenever a subband crosses from one energy box (the intervals of the discretization scheme) of the discretized energy grid to another box leading to a discontinuity in the derivatives w.r.t. the potential. Thus, any plot depicting an observable versus a contact bias – or any other quantity that influences the potential within the device – will exhibit these kinds of discontinuities to some degree if the H-transformation has been used.

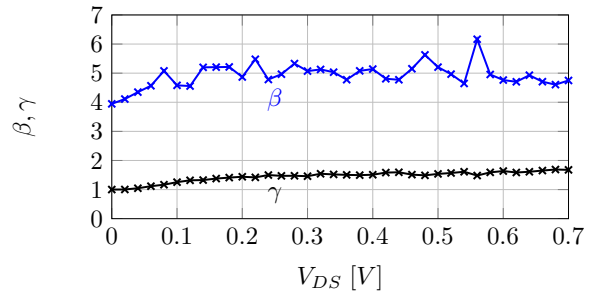

Fig. 7. Gate excess noise factor β (blue) and drain excess noise factor γ (black) vs. drain bias at $V_{GS} = 0.7V$ in the low frequency limit.

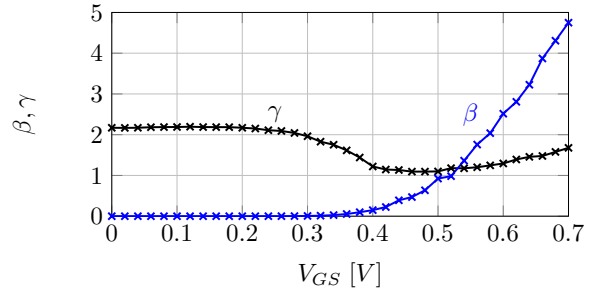

Fig. 8. Gate excess noise factor β (blue) and drain excess noise factor γ (black) vs. gate bias at $V_{DS} = 0.7V$ in the low frequency limit.

Although stationary quantities like the density and the current do in fact show the same behavior, the effect is so miniscule that it can't be seen on scales of interest. On the other hand, small signal parameters (and noise) present the discontinuities more prominently since their solution is strongly influenced by the derivatives of the BE w.r.t. the potential. Due to the origin of the discontinuities as artifacts of discretization in energy space, we can minimize their impact by choosing a finer energy grid.

B. *Microscopic Noise*

From the microscopic noise computation, we obtain PSDs that have been verified to fulfill the Nyquist theorem in equilibrium. With the PSDs and the admittance parameters, we can compute all relevant figures of merit.

In Fig. 7, we show the gate and drain excess noise factors of Eq. (2) versus the drain bias. Note how the drain excess noise factor γ immediately increases from its equilibrium value. It is known that the drain excess noise factor is larger than unity for small devices [18] compared to long channel devices where it decreases and approaches a value of $2/3$ for high drain biases [16]. Our simulation yields that the drain excess noise factor reaches a maximum at $V_{DS} = 0.7V$ of $\gamma \approx 1.68$.

In Fig. 8, the excess noise factors are plotted against the gate bias for $V_{DS} = 0.7V$. Here we find that γ is approximately constant below $V_{GS} \approx 0.2$. For higher gate biases we find qualitatively the same behavior as was found in Ref. [19] for a 180nm device.

The gate excess noise factor β becomes significantly larger than the classical long channel estimation of $4/3$ in saturation [16]. While the dependence of β on the drain bias is

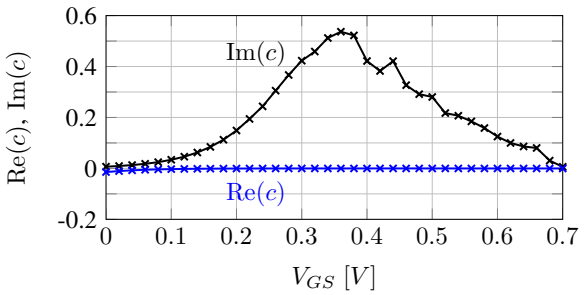

Fig. 9. Real (blue) and imaginary part (black) of cross-correlation vs. gate bias at $V_{DS} = 0.7V$ in the low frequency limit.

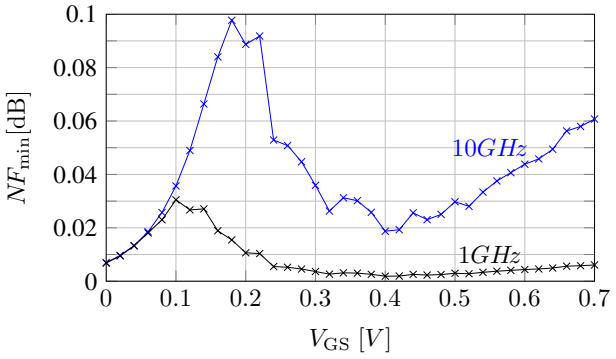

Fig. 10. Minimum noise figure in decibel, $NF_{\min}$, vs. gate bias at $V_{DS} = 0.7V$ for $1GHz$ (black) and $10GHz$ (blue).

small, we can see that it strongly depends on the gate bias in Fig. 8.

In Fig. 9, we show the real and imaginary parts of the cross-correlation of Eq. (1) plotted against the gate bias. As usual for MOSFETs, the real part of the cross-correlation is negligibly small [20] and hence it is often ignored in the noise characterization. The imaginary part has a maximum around $V_{GS} \approx 0.35V$ of approximately 0.54. This is somewhat larger than the long-channel value of 0.395 [16]. However, the imaginary part tapers off for higher gate biases and eventually approaches zero, i.e. gate and drain current fluctuations become completely uncorrelated.

The noise figure describes the degradation of the signal-to-noise-ratio when a signal passes through a two-port. Figure 10 shows the minimum noise figure $F_{\min}$. We can clearly see a local minimum around $V_{GS} = 0.4V$ where the operation of an amplifier would be optimal w.r.t. noise.

IV. Conclusion

We used a semi-classical and deterministic simulator to compute fully self-consistent small signal and noise quantities of a nanoscale double-gate nMOSFET. The solver is stable for a wide range of bias conditions and frequencies and we are able to extract key quantities for circuit designers.

We discovered discontinuities in the derivatives with respect to the potential that impact the smoothness of our results. They originate at the discretization of the energy grid in conjunction with the H-transformation and can thus be mitigated by a finer energy grid.

Our results clearly demonstrate the capabilities and the potential for applications of deterministic solvers for small signal and noise simulations.

Acknowledgment

Funding by the Deutsche Forschungsgemeinschaft (Ref. No.: JU406/9-1, ME1590/7-1) is gratefully acknowledged.

References

[1] L. Lucci, P. Palestri, D. Esseni, L. Bergagnini, and L. Selmi, "Multi-subband Monte Carlo study of transport, quantization, and electron-gas degeneration in ultrathin SOI n-MOSFETs," *Electron Devices, IEEE Transactions on*, vol. 54, pp. 1156–1164, 2007.

[2] D. Ruić and C. Jungemann, "Numerical aspects of noise simulation in MOSFETs by a Langevin-Boltzmann solver," *Journal of Computational Electronics*, vol. 14, no. 1, pp. 21–36, 2015.

[3] A. Gnudi, D. Ventura, G. Baccarani, and F. Odeh, "Two-dimensional MOSFET simulation by means of a multidimensional spherical harmonics expansion of the Boltzmann transport equation," *Solid–State Electron.*, vol. 36, no. 4, pp. 575 – 581, 1993.

[4] S.-M. Hong, A. T. Pham, and C. Jungemann, *Deterministic solvers for the Boltzmann transport equation*. Computational Microelectronics, Wien, New York: Springer, 2011.

[5] C. Herring and E. Vogt, "Transport and deformation-potential theory for many-valley semiconductors with anisotropic scattering," *Phys. Rev.*, vol. 101, no. 3, pp. 944–962, 1956.

[6] D. Esseni, P. Palestri, and L. Selmi, *Nanoscale MOS Transistors. Semi-Classical Transport and Applications*. Cambridge University Press, 2011.

[7] R. E. Prange and T. W. Nee, "Quantum spectroscopy of the low-field oscillations in the surface impedance," *Phys. Rev.*, vol. 168, pp. 779–785, 1968.

[8] H. Kosina, "A method to reduce small-angle scattering in Monte Carlo device analysis," *Electron Devices, IEEE Transactions on*, vol. 46, no. 6, pp. 1196–1200, 1999.

[9] D. Ruić and C. Jungemann, "A self-consistent solution of the Poisson, Schrödinger and Boltzmann equations by a full Newton-Raphson approach for nanoscale semiconductor devices," in *Simulation of Semiconductor Processes and Devices (SISPAD), 2013 International Conference on*, pp. 356–359, Sept 2013.

[10] S. Kogan, *Electronic Noise and Fluctuations in Solids*. Cambridge, New York, Melbourne: Cambridge University Press, 1996.

[11] F. H. Branin, "Network sensitivity and noise analysis simplified," *IEEE Transactions on circuit theory*, vol. 20, pp. 285–288, 1973.

[12] W. Shockley, "Currents to conductors induced by a moving point charge," *J. Appl. Phys.*, vol. 9, pp. 635–636, 1938.

[13] S. Ramo, "Currents induced by electron motion," *Proc. IRE*, vol. 27, pp. 584–585, 1939.

[14] H. Kim, H. S. Min, T. W. Tang, and Y. J. Park, "An extended proof of the Ramo-Shockley theorem," *Solid–State Electron.*, vol. 34, pp. 1251–1253, 1991.

[15] H. Rothe and W. Dahlke, "Theory of noisy fourpoles," *Proc. IRE*, vol. June, pp. 811–818, 1956.

[16] A. van der Ziel, *Noise in Solid State Devices and Circuits*. Canada: John Wiley and Sons, 1986.

[17] F. M. Klaassen and J. Prins, "Thermal noise of MOS transistors," *Philips Res. Repts*, pp. 505–514, 1967.

[18] A. J. Scholten, L. F. Tiemeijer, R. van Langevelde, R. J. Havens, A. T. A. Z. van Duijnhoven, and V. C. Venezia, "Noise modeling for RF CMOS circuit simulation," *Electron Devices, IEEE Transactions on*, vol. 50, no. 3, pp. 618–632, 2003.

[19] C. Jungemann, B. Neinhüs, C. D. Nguyen, A. J. Scholten, L. F. Tiemeijer, and B. Meinerzhagen, "Numerical modeling of RF noise in scaled MOS devices," *Solid–State Electron.*, vol. 50, pp. 10–17, 2006.

[20] A. van der Ziel, "Gate noise in field effect transistors at moderately high frequencies," *Proc. IEEE*, vol. 51, no. 3, pp. 461–467, 1963.